www.amlett.com, www.vbripress.com/aml, DOI: 10.5185/amlett.2015.5656 Published online by the VBRI press in 2015

Effect of synthesis time on structural, optical and electrical properties of CuO nanoparticles synthesized by reflux condensation method

N. Bouazizi[1*], R. Bargougui[2], A. Oueslati[3], R. Benslama[1]

[1]*Environment, catalysis and analysis methods laboratory, ENIG University of Gabes, Tunisia.*
[2]*Faculty of Sciences of Gabes, Cite Erriadh, 6072, University of Gabes,Tunisia*
[3]*Solid Laboratory, Faculty of Sciences of Sfax, Tunisia*

[*]Corresponding author. E-mail: bouazizi.nabil@hotmail.fr

Received: 09 August 2014, Revised: 05 November 2014 and Accepted: 15 November 2014

ABSTRACT

CuO nanopowder oxide was synthesized by reflux condensation method without any surfactants or templates, using copper nitrate in deionized water and aqueous ammonia solution. The structural, optical and electrical properties of the sample were investigated using X-ray diffraction (XRD), FT-IR, UV–visible spectroscopy and impedance spectroscopy measurements. The X-ray diffraction patterns revealed that CuO nanoparticles (NPs) was formed in pure monoclinic phase and good crystalline quality, whose NPs sizes were of the order 25 nm which an average size can be tailored by the synthesis time. FT-IR spectra of CuO NPs used to detect the possible adsorbed species on the CuO materials. In addition, the peaks at 529 and 604 cm^{-1} correspond to the characteristic stretching vibrations of Cu-O bond in the monoclinic CuO. The optical absorption property has been determined by UV–visible Spectroscopy in the wavelength range of 200–800 nm which indicate the energy gap (Eg). As result, Eg increases with increasing the synthesis time from 2.72 to 1.87 eV. The complex measurement has been investigated at room temperature, and in the frequency range 40 Hz–100 kHz, showing that Nyquist plots (Z' versus Z") are well fitted to an equivalent circuit model which consists of a parallel combination of a bulk resistance R_b and constant phase elements CPE. On the other hand, the capacitance and the conductance of CuO NPs have a proportional relationship to the charge transfer and the surface electrode-pallet. These properties make these materials very promising electrode.

Keywords: CuO; synthesis time; electrical properties; band gap; nanoparticles.

Nabil BOUAZIZI is doctoral Research Fellow in Chemistry at Environment, catalysis and analysis methods laboratory, ENIG, University of Gabes, Tunisia. His research interests are in nanomaterials, metal oxide, carbon dioxide adsorbents, hydrogen production and sensors.

Radhouane BARGOUGUI is a doctoral Research Fellow in Chemistry at Faculty of Sciences of Gabes, Cite Erriadh, 6072, University of Gabes, Tunisia. His research Interests are electrochemical study of nanomaterials, AC conductivity of metal oxide and their applications.

Introduction

Copper oxide (CuO) has attracted much attention in recent years because of its promising applications such as CuO is an attractive p-type metal oxide semiconductor that has unique electrical, optical and catalytic properties, solar cells, gas sensors **[1-4]**. CuO is widely used in electrochemical cells **[4]**, gas sensors **[5–7]**, magnetic storage media **[8, 9]**, photovoltaic cells **[10]**, light emitters **[11]**, thermoelectric materials **[12, 13]**.

Among these CuO nanostructures, the formation of CuO nanowires and nanoparticles has been extensively studied by using several techniques, such as precursors **[14]**, hydrothermal decomposition **[15]**, self-catalytic growth **[16]** and solvothermal **[17]** routes. Cupric Oxide having monoclinic structure is a unique monoxide compound for both fundamental investigations and practical applications. Using CuO nanoparticles with narrow size distribution for these applications would further promote the chemical reactivity of the nanoparticles because as the particle's size reduces the surface-to- volume ratioin creases,and

consequently the number of reactive sites increases **[18–22]**.

The p-type semiconductor of copper oxide (CuO) is an important functional material used for gas sensors, magnetic storage media, solar energy transformation, electronics, semiconductors, varistors, and catalysis. It has therefore been studied together with other copper oxides, especially with respect to its applications as a photo thermally active and photoconductive compound **[23]**.

CuO reveal Narrow band-gap p-type semiconductor between 1.2 and 1.5 eV, wish have been particularly interesting because of their promising for electronic and optoelectronic devices. CuO is a key component in high superconductors and is also used as a photoconductive material. Owing to its photochemical properties, CuO has been widely used in the fabrication of anode material for Li-ion battery **[24, 25]**.

In this paper CuO NNPs were synthesized using the reflux condensations approach without the assistance of surfactants or organic solvents has been introduced as a simple synthesis method of fundamentally important well-defined nanometer-sized materials under mild conditions. Even though some studies concerning the formation of CuO NNPs via various kinds of methods have been reported **[26–29]**, studies on the formation of the CuO NNPs have been performed.

In addition, the structural, optical, electrical properties were investigated by X-ray diffraction (XRD), Fourier transform infrared spectroscopy (FTIR), UV-Vis. Also, the several of the NNPs size nanostructures were demonstrated to evaluate the structural parameter of CuO. The variation of the optical behavior as a function of CuO NNPs size has been investigated in this work.

Experimental

Synthesis of CuO nanopowder

CuO nanopowders were prepared by simple reflux condensation method. In a typical synthesis, 0.1 mol/L of copper nitrate trihydrate ($Cu(NO)_3$ $3H_2O$) was prepared in 75 mL of deionized water under constant stirring until a homogeneous blue color solution was obtained. Then, 5 mol/L of aqueous ammonia solution was injected vigorously under constant stirring, and the resulting blend was refluxed at 80°C for 6 hours. When ammonia was injected the initial solution turned from blue color to violet color and as the time proceeds the solution further turned to black color indicating the formation of CuO. The product was cooled to room temperature naturally, and the black precipitate was obtained by centrifugation and washed with methanol several times to remove the remnant ions. Finally, the black product was dried in air at 80°C for 4 hours.

Characterization and impedance analysis:

X-ray diffraction spectra were carried using a Bruker D8-Advance diffractometer equipped with a source delivering a monochromatic Cu $K\alpha_1$ radiation (λ = 1.54056 Å), with step size 0.02. Infrared spectra were recorded using a KBr cell Fourier transformed IR equipment and infrared spectroscopy (NICOLET IR200), of wave ranged from 4000 to 400 cm^{-1}. Each sample was scanned 40 times for spectrum integration, and scanning resolution was 2 cm^{-1}. Different methods of implementation allow us to have information on the solution UV-VISIBLE spectrophotometer (SHIMADZU, UV-1650PC). A pallet of CuO powder in thickness was used for the electrical measurements, where the electrical measurements of the real and imaginary components of the impedance parameters (Z' and Z") were made over a wide at room temperatures and frequencies (40 Hz–100 kHz). These measurements were performed by using a Tegam 3550 impedance analyzer.

Results and discussion

Structural and surface analysis

XRD patterns of CuO NNPs grown on copper foils for different synthesis time are shown in **Fig. 1**. Different peaks were observed at (2θ) = 32.67° (111), 35.63° (002), 38.90° ($\bar{1}11$), 48.83° ($\bar{2}02$), 53.60° (020), 58.24° (202), 61.59° ($\bar{2}13$), 66.5° (022) and 68.19° (220) corresponds to different planes of monoclinic phase of CuO (with S.G. C2/c; and lattice constants (JCPDS No. 02-1225) **[30]**.

It is clear that the major peaks located at 2θ = 35.43° and 38.49° are the characteristics peaks for the pure monoclinic phase of CuO NNPs. The sharp and narrow diffraction peaks indicate that the material has good crystallinity and no other impurities were detected. The average grain size of copper oxide is calculated by using the Scherrer formula:

$$D = 0.89\,\lambda / \beta \cos\theta \qquad (1)$$

Where D is the crystallite size, λ is the wavelength (1.5406 Å for Cu Kα), β is the full-width at half-maximum of main intensity peak after subtraction of the equipment broadening and θ is the diffraction angle. The average grain size was found to be around 20-35nm.

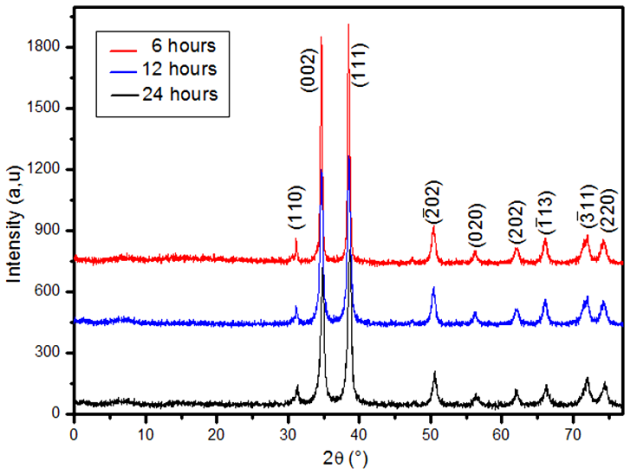

Fig. 1. XRD pattern of powder samples CuO prepared at different synthesis time.

Furthermore, increased preparation time noticed that all peaks of CuO (**Fig. 2**) are slightly shifted to higher angles indicating a small decrease in the NNPs size. More important to observe the lower peak intensity is especially in the case of prepared CuO in 24 hours. Otherwise, these

observations indicate that the change NNPs size depends on the synthesis time, which can be explained by the particles formation and stabilization.

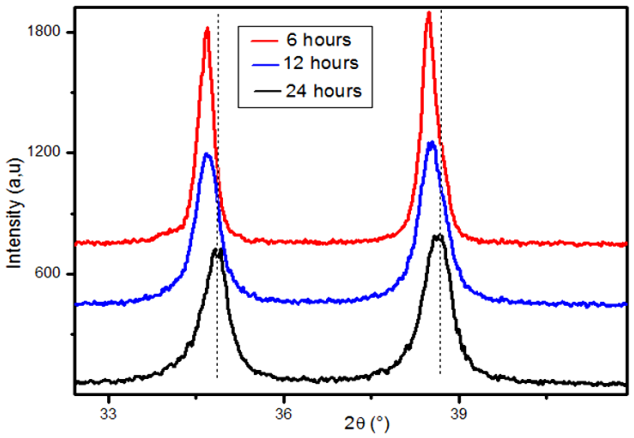

Fig. 2. Illustration of the shift of peak.

UV–vis absorption spectra and energy gap calculation

The absorption spectra of the as-synthesized samples with average synthesis time of 6, 12 and 24 hours is shown in the **Fig. 3.** The figure depicts absorption peaks at about 205, 214 and 221 nm for the three samples, respectively. Until the synthesis time of these NNPs influence on the size, this is small shift in the band gap. These facts result from can be explained, to the increase of electron concentration due to copper stabilization. With increase in the annealing synthesis time from 6 to 24 hours, the optical absorption edge slightly shifted towards longer wavelength, which may be attributed to the increase in grain size **[31, 32]**.

The optical band gap (Eg) of CuO was determined by using the formula:

$$(\alpha h\upsilon)^n = B(h\upsilon\text{-}Eg) \qquad (2)$$

Where B is a constant related to the material, hν is the photon energy in eV, h is Plank's constant, ν is the frequency of the photon, Eg is the optical band gap in eV, n is an exponent that can take a value of either 2 for direct transition or ½ for an indirect transition, and α is the absorption coefficient (in cm^{-1}) **[33, 34]**.

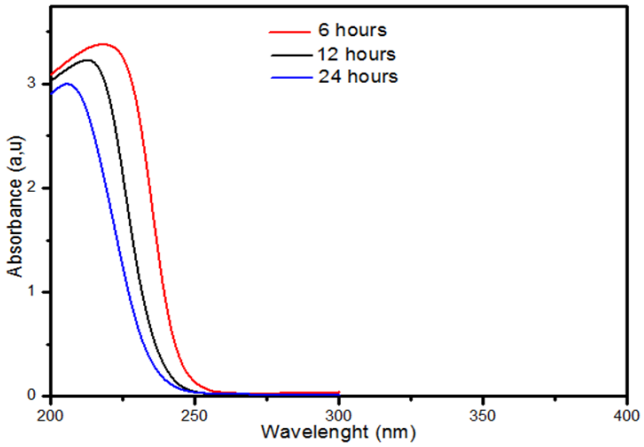

Fig. 3. UV–visible absorption spectra of colloidal CuO nanoparticles for different synthesis time.

Fig. 4 represents $(\alpha h\nu)^2$ versus hν plots for direct transition and the extrapolation of linear curve to zero absorption edge energy corresponds to band gap Eg of absorption spectra for three different synthesis time of CuO nanoparticles.

From UV–vis results, the shift in the band gap attributed to the effect of synthesis time on the crystallinity of CuO, which shows a greater shift compared with that of the bulk (1.72 eV) due to the size effect **[35]**.

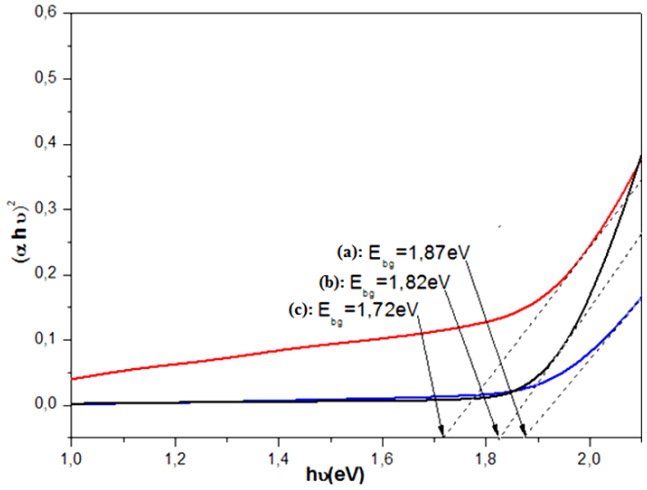

Fig. 4. Direct band gap estimations of colloidal CuO nanoparticle samples for different synthesis time: (a) 24 hours, (b) 12 hours and (c) 6 hours.

Thus, the observed shift in the optical absorption spectra with particle size reduction is a clear sign of the energy gap enlargement due to the quantum-confinement effects. In this case, the optical band gap changes in CuO samples upon increasing in synthesis time due to the change of crystallinity **[36]**.

Indeed, the band gap was found to be 1.87 eV from the UV–visible spectra which conforms CuO crystals having semiconductor character, where they obtained direct band gap values are depends on the size and the synthesis time of NNPs (**Table 1**). The observed increase in the direct band gap values of CuO with the decrease in NNPs size is attributed to the quantum-confinement effect **[37, 38]**.

Table 1. Dependence of energy gap and nanoparticles size with the synthesis time.

Time (hours)	**24**	**12**	**6**
NNp size (nm)	23.025	35.04	29.58
Eg (eV)	1.87	1.82	1.72

FT-IR investigations and effect of the synthesis time

The FT-IR transmittance spectrum (**Fig. 5**) of the CuO nanopowder synthesized for different synthesis time was recorded at room temperature. The absorption bands at 430, 507, and 606 cm^{-1} have been observed which is due to the Cu-O stretching in the monoclinic phase of CuO **[39]**. This FTIR analysis confirmed that the solid powder synthesized for different synthesis time was in pure phase of CuO. Weak and broad absorption bands at 1637 and

3432 cm^{-1} have been observed due to the existence of water molecules and 1354 cm^{-1} is due to C–H stretching vibrations. No vibrations at 615–621 cm^{-1} of Cu_2O impurities were detected **[40]**.

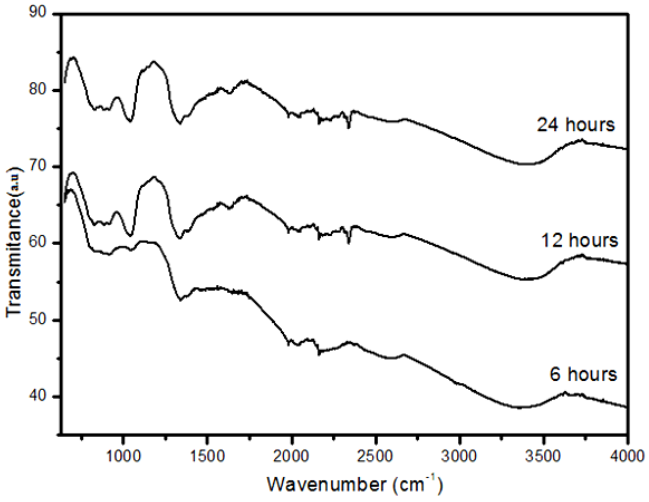

Fig. 5. FT-IR spectra of CuO nanoparticles for different synthesis time.

Fig. 6 shows that the preparation time has a significant effect on the NNPs CuO, in which the existence of an offset of 10 cm^{-1} to higher wavelengths for the same band vibration of elongations type SiO_4. This shift is explained by the effect of synthesis time, which leads to a weakening of the interaction between Cu-O. Moreover, CuO prepared in 6 hours is characterized by the absence of the band around 2350 cm^{-1} that it is very likely they are due to the synthesis time effect, which enters into the formation and stabilization of CuO NNPs.

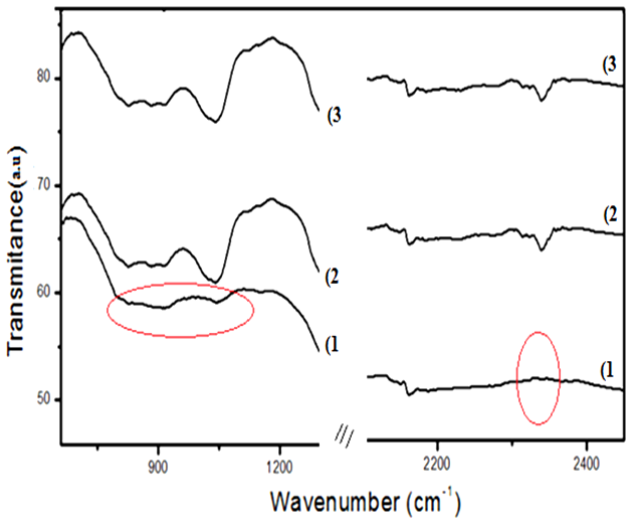

Fig. 6. Change of vibrational bands of CuO recorded for different synthesis times: 1) 6 hours, 2) 12 hours and 3) 24 hours.

Impedance analysis

Complex impedance plotting techniques can be used to differentiate conduction processes, build the equivalent circuit model and analyze the mechanism of the sensing materials **[41-44]**. The frequency range is 40 Hz–100 kHz. ReZ (Z') and ImZ (Z") are the real part and imaginary part of the complex impedance, respectively. In order to study the characteristics of our compound CuO (24 hours), the imaginary and real part of impedance is plotted in **Fig. 7**. It is Claire that the data points are located on circular arcs passing near the origin and having centers below the real axis. The arc pattern tells us about the electrical process occurring within the sample, and their correlation with the sample microstructure when modeled in terms of an electrical equivalent circuit **[45-47]**. It allows the establishment of correlations between electrochemical system parameters and impedance elements characteristics. Therefore, the complex impedance curve of this compound can be represented by the Debye model, which suggests the existence of an arc of a circle centered on the real axis, and many investigations have explained that it is due to a kind of polarization and can be modeled by an equivalent circuit of parallel resistor and capacitor **[44, 48, 49]**. This semicircle represents a kind of sensing mechanism, which is based on the conductivity of present proton, only free protons can be formed. Indeed, they can migrate by hopping from site to site across the surface.

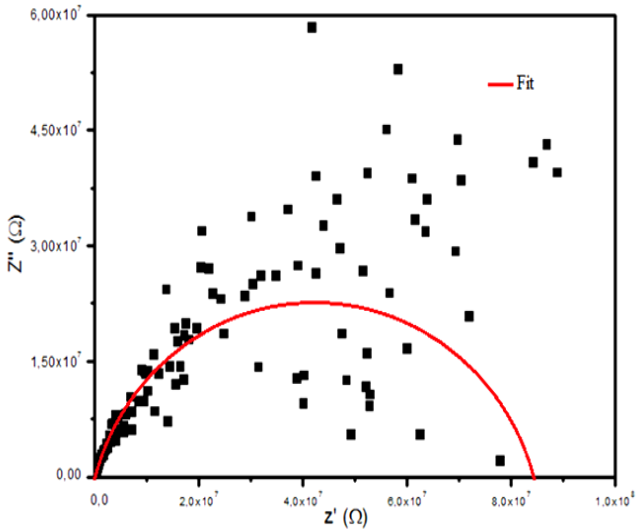

Fig. 7. Debye plots of CuO at room temperatures.

Fig. 8 (a) and **(b)** show the variation of the real (Z') and imaginary (Z") parts, where they values are high in the low frequency region. This effect is due to the accumulation of free charges at the pellet–electrolyte interface. Although, in high frequency both values tend towards values close to zero, that indicates the decrease in the dielectric constant of the material. All the curves merge in high-frequency region (>10^5 Hz), and then Z' becomes independent of frequency. Such behavior indicates the presence of relaxation in the system.

Nyquist plots reported in **Fig. 8** show a good conformity of calculated lines with the experimental data indicating that the suggested equivalent circuit describes the pellet–electrolyte interface reasonably well. **Fig. 9** shows the frequency dependence of Z' and Z" at room temperature. As the frequency increases Z" increasing whereas Z' decreases. This trend continues up to a particular frequency which in Z" occupies a maximum value and in Z' intersects. Furthermore, if the frequency increases both Z' and Z" decrease, and above 10^5 Hz both values merge with X-axis. This indicates that there exists a relaxation phenomenon.

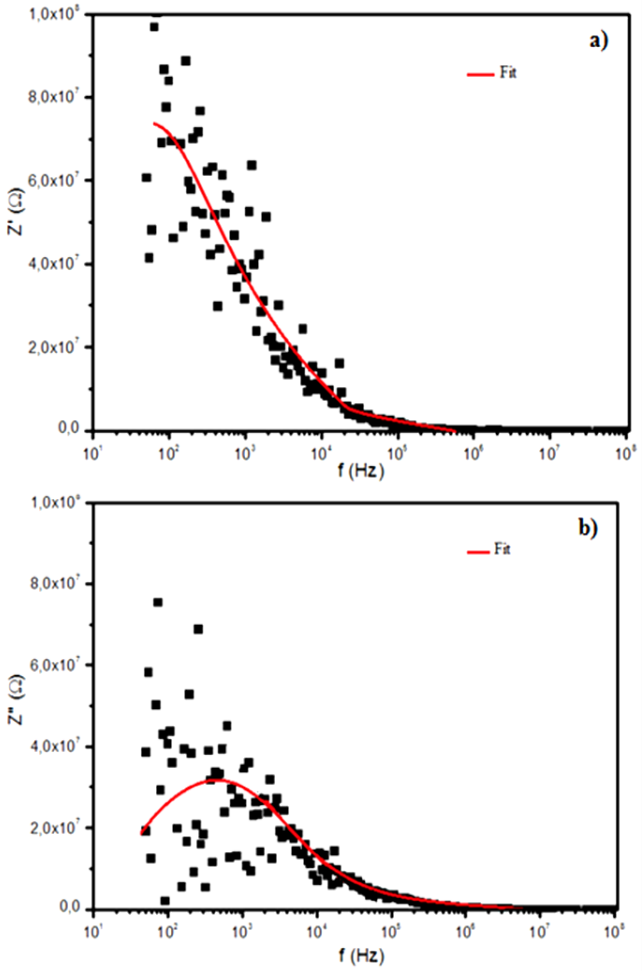

Fig. 8. Variation of real a) and imaginary b) parts of impedance as a function of frequency at room temperature.

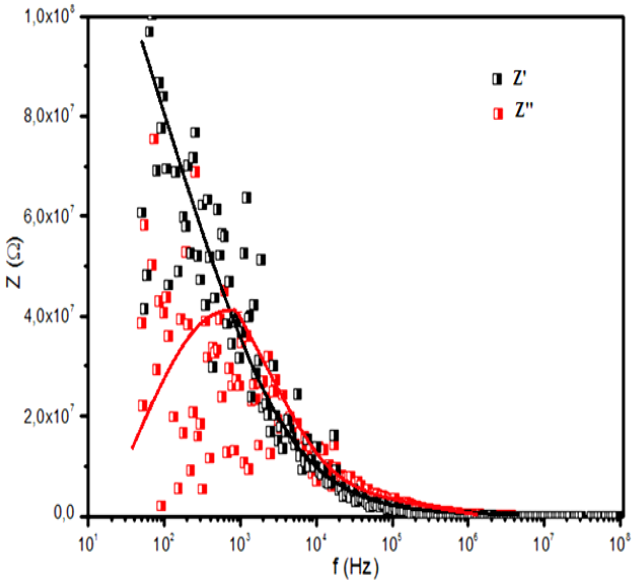

Fig. 9. Frequency dependence of Z' and Z'' for CuO.

The equivalent circuit of CuO sample (**Fig. 10**) corresponds to the parallel combination of polarization resistance Rb (bulk resistance) and a term of complex elements: constant phase elements (capacity of the fractal interface CPE) **[50]**.

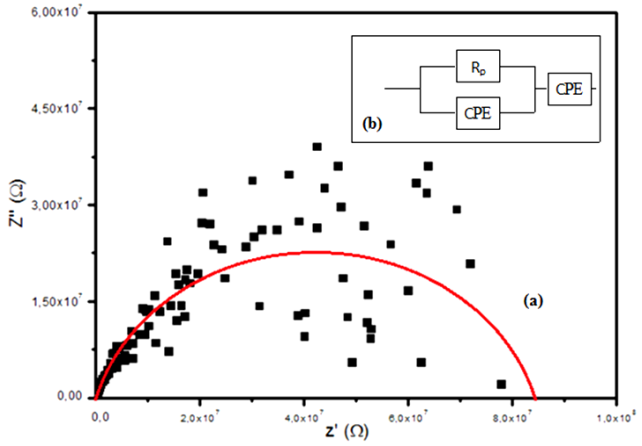

Fig. 10. (**a**) Complex plane of CuO nanoparticles at room temperature and (**b**) electrical equivalent circuit.

Frequency dependence of conductance and capacitance

The angular frequency dependence of the conductivity for the sample is shown in **Fig. 11**. In fact, the conductance curves reveal two distinct regions, the low frequency regions and high frequency regions. The variations of conductance with frequencies find that conductance increases with rise in frequency. This increase of the conductance is attributed to materials activation which allows the hopping of charged carriers between different localized states. Different conduction mechanisms (hopping, tunneling or free band) can lead to power law behaviour for the conductivity. Since, it is difficult to decide which of the mechanisms is responsible for the observed conduction properties in the CuO NPs. The evolution of frequencies dependence of the conductance value can help to explain the conduction mechanism in this sample. This provides further evidence in support of the activated conduction processing CuO **[52]**, when a sample is placed in an electrical field, electrons hop between localized sites. The charge carriers, moving between these sites hop from a donor to an acceptor state. So far, different conduction mechanisms (hopping, tunneling or free band) can lead to power law behaviour for the conductivity.

In order to investigate the different kind's effects of CuO surface functional on the capacitance, **Fig. 12** shows the capacitance–frequency characteristics of CuO NPs measured at fixed voltage. In general, the capacitance of the materials decreased with the increase in frequency. Here, the accumulation capacitance decreased and it presents fluctuation for the materials. As the frequency increases, capacitance increases, which display the applicability of the prepared samples evaluated as the active material in capacitors. As result, a significantly capacitance decreases by increasing the frequency can be attributed to the fact that at low frequencies the electrode material can be fully utilized while at higher analysis rates. The high capacitance at low frequencies depends on the ability of the charge carriers to follow the applied signal, while the decrease in capacitance at higher frequencies, the charge at the interface may not follow signal **[53, 54]**. All these results reveal the strong effect of samples stability on the capacitance performance of CuO NPs.

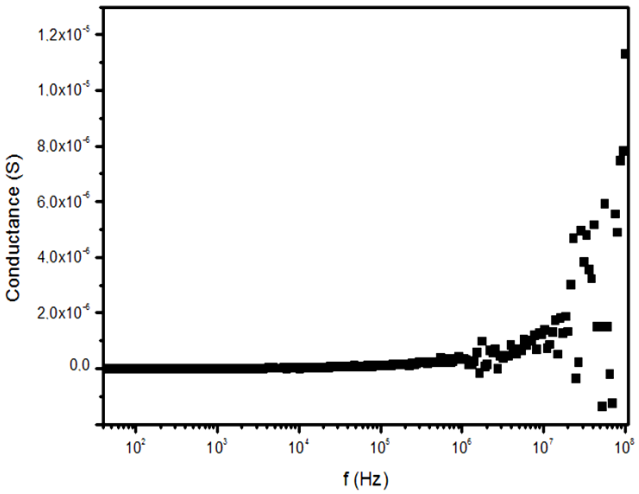

Fig. 11. Characteristics conductance- frequencies of CuO NPs.

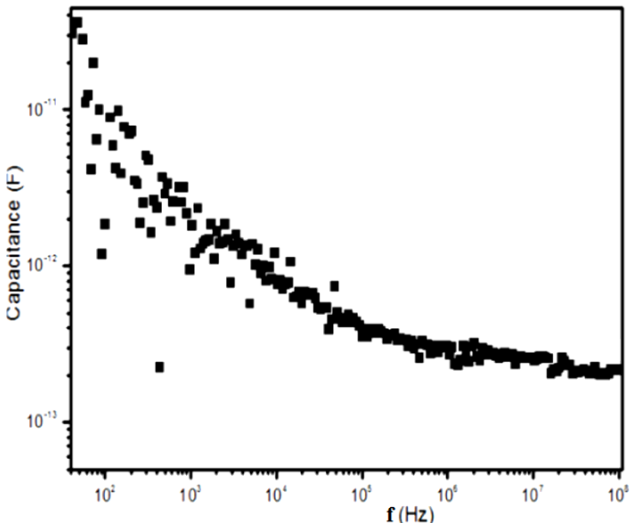

Fig. 12 Characteristics capacitance- frequencies of CuO NPs.

Conclusion

In summary, CuO nanoparticles with a monoclinic structure were successfully prepared using a reflux condensation synthesis process. The results show that the variation in the synthesis time have influence the structural and optical proprieties of CuO nanoparticles. In the UV–visible absorption, shift of band-gap energy was observed with decreasing nanoparticle size due to the synthesis time effect. This is also in agreement with the direct band gap energy calculation based on the absorption spectra which showed higher values for smaller nanoparticle size. Our experimental results demonstrated that the as prepared CuO nanoparcile has a good electrical property. Besides, Z' and Z" curves merge above 10^5 Hz at room temperature reveal the space charge polarization. These present observations can help improve our understanding of the formation and physical properties of CuO nanoparticles.

Reference

1. S.Y, Sung.; S.Y, Kim.; K.M, Jo.; J.H, Lee.; J.J, Kim.; S.G, Kim.; K.H, Chai.; S.J, Pearton; D.P, Norton.; Y.W, Heo.; *J. Appl. Phys. Lett.* **2010**, *222*, 109. **DOI:** 10.1063/1.3656974
2. Sahay, R.; Sundaramurthy, J.; Kumar, P. S.; Thavasi, V.; Mhaisalkar, S. G.; Ramakrishna, S.; *J. Solid. State. Chem.* **2012**, *261*, 267. **DOI:** 10.1021/jp3053949
3. Gao, S.; Yang, S.; Shu, J.; Zhang, S.; Li, Z.; Jiang, K.; *J. Phys. Chem. C.* **2008**, *19324*, 19328. **DOI:** 10.1039/C1JM11813G
4. Comanac, A.; Medici, L. D.; Capone, M.; Millis, A. J.; *Nat. Phys.* **2008**, *287*, 290. **DOI:** 10.1038/nphys883
5. Morales, J. ; Sanchez, L. ; Martın, F. ; Barrado, J. R. ; Sanchez, M. ; *J. Thin. Solid. Films* **2005**, 133. **DOI:** 10.10148/nphys883
6. Cruccolini, A. ; Narducci, R. ; Palombari, R. ; *J. Sens. Actuators. B.* **2004**, *98*, 227. **DOI:** 10.1016/j.snb.2003.10.012
7. Katti, V. R.; Debnath, A. K.; Muthe, K. P.; Kaur, M.; Dua, A. K.; Gadkari, S. C.; Gupta, S. K.; Sahni, V. C.; *J. Sens. Actuators. B.* **2003**, *96*, 245. **DOI:** U0026-0812200914114618
8. Frietsch, M.; Zudock, F.; Goschnick, J.; Bruns, M.; *J. Sens. Actuators. B-Chem.* **2000**, *65*, 379. **DOI:** 10.1016/S0925-4005
9. Fan, H.; Yang, L.; Hua, W.; Wu, X.; Wu, Z.; Xie, S.; Zou, B.; *Nanotechnology*. **2004,** *15*, 37. **DOI:** 10.1088/0957-4484/15/1/007
10. Mallinson, J. C.; Academic Press, Berkeley, CA (Chapter 3), **1987**. **DOI:** 10.1063/1.4810192
11. Larsson, P. O.; Andersson, A.; Wallengerg, R. L.; Svensson, B.; *J. Catal.* **1996**, *163*, 279. **DOI:** 10.2147/IJN.S29020
12. Hsieh, C. T.; Chen, J. M.; Lin, H. H.; Shih, H. C.; *J. Appl. Phys. Lett.* **2003**, *83*, 3383. **DOI:** 10.1155/2011/268508
13. Koumoto, K.; Koduka, H.; Seo, W.S.; J. Mater. Chem. **2001**, 11, 251. **DOI:** 10.1016/j.tsf.2004.08.117
14. Guan, H.; Shao, C.; Chen, B.; Gong, J.; Yang, X.; *J. Inorg. Chem.* **2003**, 1409, 1411. **DOI:** 10.1155/2011/863631
15. Chen, D.; Shen, G.; Tang, K.; Qian, Y.; *J. Cryst. Growth.* **2003**, *254*, 225. **DOI:** 10.1016/S0009-2614(03)00877-7
16. Hsieh, C. T.; Chen, J. M.; Lin, H. H.; Shih, H. C.; *J. App. Phys. Lett.* **2003**, *3316*, 3318. **DOI:** 10.1016/j.tsf.2004.08.117
17. Cao , M.; Hu , C.; Wang , Y.; Cuo, Y.; Guo , C.; Wang , E.; *J. Chem. Commun.* **2003,** *15*, 1884. **DOI:** 10.1186/1556-276X-9-624
18. Rajagopalan, S.; Koper, O.; Decker, S.; Klabunde, K.J.; *Chem. Eur. J.* **2002**, *8*, 2602. **DOI:** 10.1002/1521-3765(20020603)8:11<2602
19. Klabunde, K.J.; J. Nanoscale Materials in Chemistry, John Wiley and Sons, New- York, **2001**. **DOI:** 10.1002/0471220620.ch1
20. Klabunde, K. J.; Stark, J.; Koper, O.; Mohs, C.; Park, D. G.; Decker, S.; Lagadic, Y. J.; Zhang, D.; *J. Phys. Chem.* **1996**, *100*, 12142. **DOI:** 140204741X, 9781402047411
21. Rodriguez, J. A.; Fernandez Garcia, M.; Synthesis Properties and Applications of Oxide Nanomaterials, John Wiley and Sons, New York, **2007**. **DOI:** 10.1002/0470108975
22. Winter, M.; Hamal, D.; Yang, X.; Kwen, H.; Jones, D.; Rajagopalan, S.; Klabunde, K.J.; *J. Chem. Mater.* **2009**, *21*, 2367. **DOI:** 1461442591, 9781461442592
23. Chih-Hung, L.; Tsing-Tshih, T.; *J. Vac. Sci. Technol. B.* **2005**, *2394*, 23976. **DOI:** 10.3786/nml.v4i2.p73-77
24. Sahay, R.; Kumar, P. S.; Aravindan, V.; Sundaramurthy, J.; Ling, W. C.; Mhaisalkar, S. G.; Ramakrishna, S.; Madhavi, S.; *J. Phys. Chem. C.* **2012**, *18087*, 18092. **DOI:** 10.1021/jp3053949
25. Liu, Y.; Zhong, L.; Peng, Z.; Song, Y.; Chen, W.; *J. Mater. Sci.* **2010**, *3791*, 3796. **DOI:** 10.1155/2014/856592
26. Eliseev, A. A.; Lukashin, A. V.; Vertegel, A. A.; Heifets, L. I.; Zhirov, A. I.; Tretyakov, Y. D.; *J. Mater. Res. Innov.* **2000**, *3*, 308. **DOI:** 10.1007/PL00010877

27. Xu, J. F.; Ji, W.; Shen, Z. X.; Tang, S. H.; Ye, X. R.; Jia, D. Z.; Xin, X. Q.; *J. Solid. State. Chem.* **1999**, *147*, 516.
DOI: 10.1006/jssc.1999.8409
28. Borgohain, K.; Singh, J. B.; Rama Rao, M. V.; Shripathi, T.; Mahamuni, S.; *J. Phys. Rev. B.* **2000**, *61*, 11093.
DOI: 10.1103/PhysRevB.61.11093
29. Sawsan, Dagher.; Yousef, Haik.; Ahmad, Ayesh.; Nacir, Tit.; *J. Lumin.* **2014**, *149*, 154.
DOI: 10.1016/j.jlumin.2014.02.015
30. Powder Diffract. File, JCPDS-ICDD, 12 Campus Boulevard, Newtown Square, U.S.A PA. **2001**, *19073*, 3273.
DOI: 0885-7156 e-ISSN: 1945-7413
31. Marcano, D. C.; Kosynkin, D.V.; Berlin, J. M.; Sinitskii, A.; Sun, Z.; Slesarev, A.; Alemany, L. B.; Lu, W.; Tour, J. M.; *ACS. Nano.* **2010**, *4*, 4806.
DOI: 10.1021/nn1006368
32. Zou, G.; Li, H.; Zhang, D.; Xiong, K.; Dong, C.; Qian, Y. *; J. Phys. Chem. B.* **2006**, *1632*, 1637.
DOI: 10.1021/am201663d
33. Ahmed, A. N.; Gajbhiye, S.; Joshi, A. G.; *J. Solid. State. Chem.* **2011**, *2209*, 2214.
DOI: 10.1016/j.jssc.2011.05.058
34. Zhang, Y.; Fa, W.; Yang, F.; Zheng, Z.; Zhang, P.; *J. Ionics.* **2010**, *815*, 820.
DOI: 10.3762/bjnano.4.81
35. Shinde, V. R.; Lokhande, C. D.; Mane, R. S.; Han, S. H.; *J. Appl. Surf. Sci.* **2005**, *407*, 413.
DOI: 10.1016/j.apsusc.2004.10.036
36. Kaushal, A.; Kaur, D.; *J. Alloys. Compd.* **2011**, *200*, 205.
DOI: 10.1016/j.jallcom.2010.09.077
37. Chandrappa, K. G.; Venkatesha, T. V.; Vathsala, K.; Shivakumara, C.; *J. Nanoparticle Research.* **2010**, *2667*, 2678.
DOI: 10.1007/s11051-009-9846-0
38. Subramanian, B.; Sanjeeviraja, C.; Jayachandran, M. ; *J. Cryst. Growth.* **2002**, *421*, 426.
DOI: 10.1016/S0022-0248(01)01697-9
39. Fan, J. C.; Xie, Z.; *J. Mat. Sc. Eng. B.* **2008**, *61*, 65.
DOI: 10.1016/j.apsusc.2008.03.193
40. Dagher, S.; Haik, Y.; Ayesh, A.; Tit, N.; *J. Lumin*, **2014**, *149*, 154.
DOI: 10.1016/j.jlumin.2014.02.015
41. Yang, J. P.; Meldrum, F. C.; Fendler, J. H.; *J. Phys. Chem.* **1995**, *99*, 5500.
DOI: 0824747666, 9780824747664
42. Dellwo, U.; Keller, P.; Meyer, J. U.; *J. Sens. Actuators. B. Chem.* **1997**, *298*, 302.
DOI: 0960-1317(1997)7:3<233:AMIFNR>2.0.ZU;2-S
43. Sadaoka, Y.; Matsuguchi, M.; Sakai, Y.; Mitsui, S.; *J. Mater. Sci.* **1998**, *2666*, 2675.
DOI: 10.1016/j.snb.2008.08.036
44. Sadaoka, Y.; Matsuguchi, M.; Sakai, Y.; Aono, H.; Nakayama, S.; Kuroshima, H.; *J. Mater. Sci.* **1987**, *3685*, 3692.
DOI: 10.1007/BF01161478
45. Yeh, Y. C.; Tseng, T. Y.; *J. Mater. Sci.* **1989**, *2739*, 2745.
DOI: 10.1007/BF02385619
46. Ben Rhaiem, A.; Guidara, K.; Gargouri, M.; Daoud, A. ; *J. Alloys. Compd.* **2005**, *392*, 87.
DOI: 10.1016/j.jallcom.2004.06.030
47. Chouaib, S.; Rhaiem, A. B. ; Guidara , K.; *J. Mater. Sci*, **2011**, *915*, 920.
DOI: 10.1007/s11581-011-0546-2
48. Nadeem, M.; Akhtar, M. J.; Khan, A.Y.; *J. Sol. State. Commun.* **2005**, *134*, 431.
DOI: 10.1039/C4RA11323C
49. Traversa, E.; Gnappi, G.; Montenero, A.; Gusmano, G.; *J. Sens. Actuators. B. Chem.* **1996**, *59*, 70.
DOI: 10.4236/jst.2011.14016
50. Traversa, E.; Bearzotti, A.; Miyayama, M.; Yanagida, H. ; *J. Sens. Actuators. B. Chem.* **1995**, *714*, 718.
DOI: 10.1016/0925-4005(94)01271-I
51. Muralidharan, P.; Venkateswarlu, M.; Satyanarayana, N.; *J. Non-Cryst. Solid.* **2005**, *351*, 583.
DOI: 10.1016/j.jnoncrysol.2005.01.032
52. Chauhan, G; Srivastava, R.; Rai, V. K.; Kumar, A.; Bawa, S. S.; Srivastava, P. C.; Kamalasanan, M. N.; *J. Appl. Phys.* **2010**, *124*, 509.
DOI: 10.1016/j.synthmet.2010.04.022
53. Maiti, C.K.; Samanta, S.K.; Dalapati, G.K.; Nandi, S.K.; Chatterjee, S.; *J. Microelectron. Eng.* **2004**, *72*, 253.
DOI: 10.1016/j.sse.2004.04.012
54. Saini, K.K.; Sharma, S.D.; Kanth, C.; Kar, M.; Singh, D.; Sharma, C.P.; *J. Non-Cryst. Solids.* **2007**, *353*, 2469.
DOI: 10.1063/1.3160137